Hindawi
Scientific Programming
Volume 2022, Article ID 9242940, 12 pages
https://doi.org/10.1155/2022/9242940

Research Article

Optimization of Fuel Cell Stack Consistency Based on Multi-Model

Yijin Zeng,[1] Jian Huang ,[2] Zhiliang Wang,[2] Junxiong Li,[2] and Yahui Yi[2]

[1]*State Key Laboratory of Shale Oil and Gas Enrichment Mechanisms and Effective Development, Beijing 100000, China*
[2]*School of Mechanical Engineering, Yangtze University, Jingzhou, Hubei 434000, China*

Correspondence should be addressed to Jian Huang; 202073040@yangtzeu.edu.cn

Received 20 April 2022; Revised 10 May 2022; Accepted 17 May 2022; Published 14 June 2022

Academic Editor: Punit Gupta

With the proposal of cloud computing, fog computing, and edge computing, various simulation operations are greatly guaranteed, which benefits the multi-model operations of Matlab and CFD. This paper established the 1-D flow network model and 12 cm ∗ 8 cm 3-steady-state PEMFC model. Based on the experiment, the intake flow distribution of the cathode anode of 80 cells is simulated to obtain the maximum and minimum intake flow cell. The 3-D and steady-state single-cell model is used to calculate the cell's performance, and the performance difference between the two cells is improved by optimizing the size structure of the single cell. The results show that the best version of the cell was obtained when the values of the width and depth were 1.1 mm and 0.8 mm, and the power density difference between the two cells decreased from 5.7% to 2.1%. The voltage difference at 1000 mA·cm^{-2} current density decreases from 0.065 to 0.035 V after optimization. The intake flow extreme difference of the reactor improved significantly, and C_v was reduced by 48.7%.

1. Introduction

Proton exchange membrane fuel cell (PEMFC) has become one of the ideal energy sources in the 21st century based on the advantages of high specific power, zero emission, and low operating noise. Due to the limited output power of individual PEMFC, fuel cells are usually connected in series to form fuel cell stacks to meet the practical power requirements. The reactants provided by the stack manifold flow through the fuel cell in multiple channels in a complex flow network in the fuel cell stack. The reactant flow and pressure distribution may differ between different cells, and a single cell's heat and water management strategy is challenging to achieve. This will cause the overall performance of the fuel cell stack to decrease [1]. Therefore, it is essential for the study of reactor equilibrium.

Generally, the layout of the intake manifold of the fuel cell stack is *Z*-shaped and *U*-shaped. In the actual work process, no matter what kind of layout, there is a specific difference in the intake airflow reaching the entrance of every single cell due to the intake loss. What is worse, this difference intensifies as the power of the stack increases (the number of cells increases). Finally, the difference in the intake airflow between the monomers will affect their electrochemical performance. The durability and implementation of the stack will be directly related to the performance of the monomer, which is a typical "bucket effect" [2]. At present, to accelerate the commercialization of fuel cells, many domestic and foreign scholars have done a lot of research on the consistency of the stack. For the consistency of the stack, the industry generally uses the voltage difference coefficient (C_v) to express [3]. The factors that affect the consistency of the stack are usually gas pressure, gas mass flows [4], control methods such as purge mode [5, 6], cell voltage detection level [1, 7], and other factors.

In summary, the research on the consistency of the stack is focused on how to improve its consistency through external factors. Because of this, this article will start from the optimization of the flow field size of the single cell and combine it with the data on the airflow distribution of the stack composed of 80 single cells. Take the highest air intake monomer and the lowest air intake monomer as a comparison, optimize the size of the flow field, and minimize the electrochemical performance differences between the two to improve the consistency of the stack. In addition, the industry's approach to optimizing the size of a single unit mainly starts from the

aspects of length [8, 9], depth [10, 11], width [12], and cross-sectional shape [13, 14]. Since the stack size of the article has been fixed and the cell adopts the cathode and anode straight flow field, the article will optimize the cell performance from the width and depth of the flow field.

2. Models and Parameters

The paper includes two models: 1-D fuel cell stack and 3-D and steady-state fuel cell monomer straight flow field model. The model and relevant parameters are as follows.

2.1. 1-D Fuel Cell Stack Model

2.1.1. Computational Domain of 1-D Model. The computational domain of the one-dimensional model is mainly used to represent the flow distribution of individual units in a stack, which is a schematic diagram of simplified stack flow network configuration. Figure 1 shows the current research situation of the fuel cell stack, including the inlet, outlet, manifold, and gas flow channel of the fuel cell stack. In this diagram, the reactants are supplied and transported at the reactor inlet of the top manifold. In this figure, the reactants are supplied at the stack inlet of the top manifold and transported along the top manifold while being assigned to the cell channel. The remaining reactants and products of the electrochemical reaction are discharged into the bottom manifold at the channel outlet and then removed from the fuel cell stack at the fuel cell stack outlet. Traffic network construction and analysis are based on controlling the volume, the i circuit shown in Figure 1. Each loop has six branches (control volume), and the top branch is a segment of the top manifold connecting adjacent units. The bottom branch is a segment of the base manifold. Each channel is divided into two branches of the same length. Branches in the circulation are numbered clockwise from the top manifold branches. Furthermore, branches in the circulation are numbered clockwise from the full manifold branches.

In this model, the pressure, velocity, and components are assumed to be uniform on each loop branch. The reaction points indicated by the symbol $\otimes$ are located in the middle of the channel, where property parameters such as pressure and flow velocity are the mean of the anterior segment and terminal channel branches. Since the mass transfer of the electrochemical reaction is considered to occur in the reaction center, the interface connecting the various branches and the different branches is represented by nodes with 4 nodes per cycle. The parameters of the reactor model are shown in Table 1.

2.1.2. Governing Equation of 1-D Model. The mathematical model of the 1-D model mainly includes the mass conservation model and the momentum conservation model, as detailed in the literature, and the specific equations are shown in Table 2.

The meanings of the corresponding letters in Table 2 are shown in Table 3.

2.2. 3-D Fuel Cell CFD Model

2.2.1. Computational Domain of 3-D Model. The physical model of the 3-D model is mainly a 12 cm ∗ 8 cm straight flow field PEMFC single cell model, as shown in Figure 2, and model parameters are shown in Table 4.

2.2.2. Assumptions of 3-D Model. This article model carries out the following assumptions:

(1) The PEMFC is operating at a steady state.
(2) The gas flow in the FF is regarded as the laminar of an ideal gas and the incompressible flow.
(3) All gases cannot pass through the proton exchange membrane.
(4) The gravity effect is neglected.
(5) Both the GDL and CL are assumed to be homogeneous and isotropic.
(6) The PEMFC model is applied in a fuel cell.

2.2.3. Governing Equation of 3-D Model. The 3-D model mainly includes mass conservation equation, momentum conservation equation, energy conservation equation, component conservation equation, electrochemical equation, diffusion equation of gas components in porous medium, and transport equation for liquid water. The specific equations are shown in Table 5.

The meanings of the corresponding source items and the letters in Table 5 are shown in Tables 6 and 7, respectively.

2.3. Validation of the Model

2.3.1. 1-D Model Validation. Figure 3 shows the comparison of the pressure drop of the numerical analysis and experimental results [15] at the anode of the PEM fuel cell stack under the same operating conditions. In Figure 3, (a) and (b) are the contrasts of the stoichiometric ratios of 1.2 and 1.5, respectively. The results show that the pressure drop obtained by the numerical method is in good agreement with the experimental results in anodic stoichiometry. Consequently, the correctness of the model is demonstrated.

2.3.2. 3-D Model Validation. To ensure the accuracy and scientificity of the simulation results, it is necessary to verify the selected model mentally, and the comparison between the experiment and the simulated polarization curve is selected as the verification method. To ensure the accuracy of the trial validation effect of the selected model, the experiment is consistent with the critical parameters in the

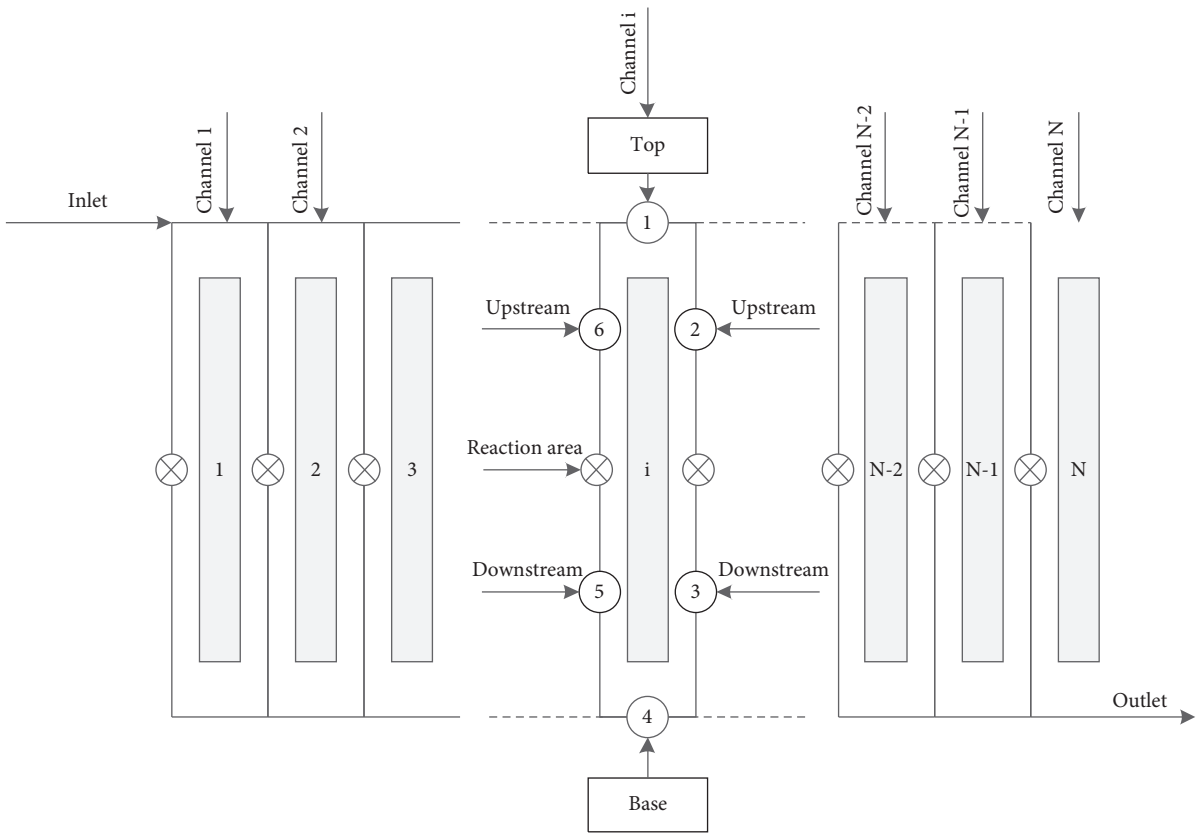

Figure 1: Geometric model of flow channel.

Table 1: Stack model parameters.

Parameter	Unit	Value
Cell number	Stretch	80
Intake manifold length	cm	12
Intake manifold width	cm	10
Intake pressure of cathode	MPa	0.2
Intake pressure of anode	MPa	0.2
Air power viscosity	$Pa{\cdot}s^{-1}$	$2.06e-5$
Hydrodynamic viscosity	$Pa{\cdot}s^{-1}$	$1.12e-5$
Flow channel section length	mm	1
Flow channel section width	mm	1
GDL thickness	um	235
Catalytic layer thickness	um	6
Membrane thickness	um	18
Channel length	cm	12
Current density	$mA{\cdot}cm^{-1}$	1000
Cathodic stoichiometric ratio	Initial	2.5
Anodic stoichiometric ratio		2.5
The cathode flow channel form	Straight	
The anode flow channel form	Straight	
Intake manifold structure	Z	

Table 2: Mass conservation and energy conservation equations of 1-D model.

Description	Equations
Inlet molar flow rate	$\dot{N}^{\text{stack}}_{\text{H}_2,\text{in}} = S_{\text{an}} N_{\text{cell}} \text{JA}_{\text{cell}}/2F$
	$\dot{N}^{\text{stack}}_{\text{O}_2,\text{in}} = S_{\text{ca}} N_{\text{cell}} \text{JA}_{\text{cell}}/4F$
Total inlet molar quality	$\dot{N}^{\text{stack}}_{\text{in,an}} = \dot{N}^{\text{stack}}_{\text{H}_2,\text{in}} \cdot P^{\text{stack}}_{\text{in,an}}/P^{\text{stack}}_{\text{in,an}} - P_{\text{sat,in}}$ $P_{\text{sat}} = e^{(77.3450+0.0057\cdot T-(7325.0/T))}/T^{8.2}$
Reaction consumption	$\dot{N}^{\text{stack}}_{\text{in,ca}} = \dot{N}^{\text{stack}}_{\text{Air,in}} \cdot P^{\text{stack}}_{\text{in,ca}}/P^{\text{stack}}_{\text{in,ca}} - P_{\text{sat,in}}$
	$\Delta\dot{N}_r = \sum_{i=\text{species}} \Delta\dot{N}^i_r$
Total molar consumption	$\Delta\dot{N}^{\text{H}_2}_r = -(\text{JA}_{\text{cell}}/2F)\Delta\dot{N}_r = \Delta\dot{N}^{\text{H}_2}_r + \dot{N}^{\text{H}_2\text{O}}_{\text{drag}}$
Molar fraction of water	$Y^{\text{H}_2\text{O}}_{\text{out,an}} = P_{\text{sat,out}}/P^{\text{stack}}_{\text{out,an}}$
Outlet molar flow rate	$\dot{N}^{\text{stack}}_{\text{H}_2,\text{out}} = (S_{\text{an}} - 1)N_{\text{cell}}\text{JA}_{\text{cell}}/2F$
	$\dot{N}^{\text{stack}}_{\text{O}_2,\text{out}} = (S_{\text{ca}} - 1)N_{\text{cell}}\text{JA}_{\text{cell}}/4F$
Flow rate of water	$\dot{N}^{\text{stack}}_{\text{H}_2\text{O,in}} = \dot{N}^{\text{stack}}_{\text{in,an}} \cdot P_{\text{sat,in}}/P^{\text{stack}}_{\text{in,an}} \dot{N}^{\text{stack}}_{\text{H}_2\text{O,out}} = T^{\text{H}_2\text{O}}_{\text{out,an}} \cdot \dot{N}^{\text{stack}}_{\text{H}_2,\text{out}}/(1 - Y^{\text{H}_2\text{O}}_{\text{out,an}})$
Water drag	$\dot{N}^{\text{stack}}_{\text{H}_2\text{O,drag}} = \dot{N}^{\text{stack}}_{\text{H}_2\text{O,in}} - \dot{N}^{\text{stack}}_{\text{H}_2\text{O,out}}$
The amount of water drag	$\dot{N}^{\text{H}_2\text{O}}_{\text{drag}} = \dot{N}^{\text{stack}}_{\text{H}_2\text{O,drag}}/N_{\text{cell}}$
Cathode water produced	$\Delta\dot{N}^{\text{O}_2}_r = -(\text{JA}_{\text{cell}}/4F)$
	$\Delta\dot{N}^{\text{H}_2\text{O}}_r = \text{JA}_{\text{cell}}/2F$
Amount of total molar mass change	$\Delta\dot{N}^{\text{ca}} = \Delta\dot{N}^{\text{O}_2}_r + \Delta\dot{N}^{\text{H}_2\text{O}}_r + \Delta\dot{N}^{\text{H}_2\text{O}}_{\text{drag}}$
The flow directions and molar flow rates for each segment	$\dot{N}_{i-1,3} = \theta_{i-1,2}\dot{N}_{i-1,2} + \Delta\dot{N}_{i-1}/\theta_{i-1,3}$
	$\dot{N}_{i,1} = \theta_{i-1,1}\dot{N}_{i-1,1} + \dot{N}^{\text{stack}}_{\text{inlet}} - \theta_{i-1,2}\dot{N}_{i-1,2}/\theta_{i,1}$
Total pressure drop	$\dot{N}_{i,4} = \theta_{i-1,3}\dot{N}_{i-1,3} - \theta_{i-1,4}\dot{N}_{i-1,4} - \dot{N}^{\text{stack}}_{\text{outlet}}/\theta_{i,4}$
	$\sum_{j=1}^{N_{\text{branch}}} \theta_{i,j}\Delta P_{i,j} = 0\,(i = 1, 2, , \ldots, N_{\text{loop}})\Delta P_{i,j} = \Delta P_{f,i,j} + \Delta P_{m,i,j}\Delta P_{f,i,j} = C_{f,i,j}L_{i,j}/D_{j,i,j}\rho_{i,j}V^2_{i,j}/2$
The calculation of Reynolds number	$C_{f,i,j} = \begin{cases} C_1 \cdot \text{Re}^{-1}_{i,j} \text{Re}_{i,j} \le 2 \times 10^3 \\ 0.316\text{Re}^{-1/4}_{i,j} 4 \times 10^3 < \text{Re}_{i,j} \le 10^5 \end{cases} \text{Re}_{i,j} = \rho_{i,j}V_{i,j}D_{h,i,j}/\mu_{i,j}$
The molar flow representation	$\Delta P_i = \sum_{j=1}^{N_{\text{branch}}} \theta_{i,j}[r_{1,i,j}\dot{N}^{n_{1,i,j}}_{i,j} + (r_{2,i,j} + r_{3,i,j})\dot{N}^{n_{2,i,j}}_{i,j}] = 0\,(i = 1, 2, 3, \ldots, N_{\text{loop}}),$
	$r_{1,i,j} = \begin{cases} 0.032L_{i,j}\mu_{i,j}\text{RT}/D^4_{h,i,j}P_{i,j} \\ 1.3560 \times 10^{-6}L_{i,j}\mu^{0.25}_{i,j}\rho^{0.75}_{i,j}(\text{RT})^{1.75}/D^{4.75}_{h,i,j}P^{1.75}_{i,j} \end{cases}$

Table 3: Meanings of symbols.

Symbol	Meaning	Symbol	Meaning
$\dot{N}$	Molar flow rate	in	Inlet of the stack
$\dot{N}_r$	Reactant consumption rate	out	Outlet of the stack
N_{cell}	Number of cells	an	Anode
A_{cell}	Active cell area	ca	Cathode
S	Stoichiometry	sat	Saturation
J	Current density	drag	Dragged molecules
P	Pressure	H_2	Hydrogen
T	Temperature	O_2	Oxygen
Y	Molar fraction	H_2O	Water
C	Wall friction coefficient	branch	Number of segments in a loop
ρ	Density	μ	Viscosity
V	Flow velocity	r	Flow resistance coefficient
D_h	Hydraulic diameter	R	Universal gas constant

simulation. Figure 2 shows the 16-channel straight flow field PEMFC used in the model simulation and experiment. Figure 4 shows the experimental schematic (the size parameters and operating parameters of the single cell in the experiment are shown in Table 8), and Figure 5 shows the polarization curve comparison of simulation and experiment. It can be seen from Figure 6 that the experimental results are consistent with the simulation results, and the

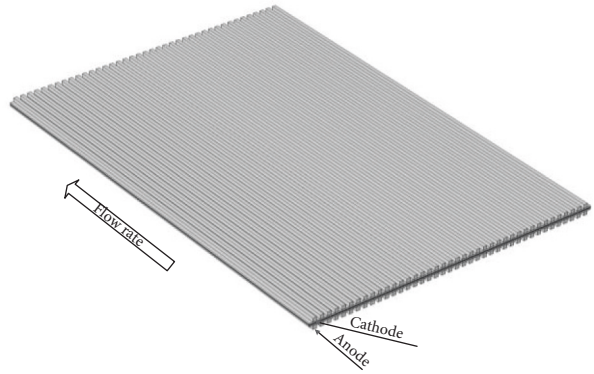

Figure 2: Geometric model of flow channel.

Table 4: Parameters of the model.

Symbol	Parameters	Value
L	Flow field length/m	0.032
W_ch	Flow field width/m	0.032
H_gdl	GDL thickness/m	$3.80e-04$
H_gdl	GDL thickness/m	$3.80e-04$
H_electrode	Porous electrode thickness/m	$5.00e-05$
H_membrane	Membrane thickness/m	$1.00e-04$
RHa	Relative humidity of anode	0.8
RHc	Relative humidity of cathode	0.8
P_sat	Saturated vapor pressure/Pa	According to calculate
P_a	Anode pressure/Pa	$2.5e5$
P_c	Cathode pressure/Pa	$2.5e5$
MH2	Hydrogen molar mass/kg·mol^{-1}	0.002
MH_2O	Water molar mass/kg·mol^{-1}	0.018
MO_2	Oxygen molar mass/kg·mol^{-1}	0.032
MN_2	Nitrogen molar mass/kg·mol^{-1}	0.028
xH_2Oa_in	Anode water vapor pressure/Pa	RHa ∗ P_sat/P_a
xH_2_in	Anode hydrogen pressure/Pa	1-xH_2Oa_in
xH_2Oc_in	Cathode water vapor pressure/Pa	RHc ∗ P_sat/P_c
xO_2_in	Cathode oxygen pressure/Pa	0.21 ∗ (1-xH_2Oc_in)
xN_2_in	Cathode nitrogen pressure/Pa	0.79 ∗ (1-xH_2Oc_in)
$D\_H_2\_H_2O$	H_2-H_2O binary diffusion coefficient/m^2·s^{-1}	$1.11e-4$ (calculated)
$D\_N_2\_H_2O$	N_2-H_2O binary diffusion coefficient/m^2·s^{-1}	$3.09e-5$ (calculated)
$D\_O_2\_N_2$	O_2-N_2 binary diffusion coefficient/m^2·s^{-1}	$2.89e-5$ (calculated)
$D\_O_2\_H_2O$	O_2-H_2O binary diffusion coefficient/m^2·s^{-1}	$3.41e-5$ (calculated)
mu_anode	Anode viscosity/Pa·s	$1.19e-05$
mu_cathode	Cathode viscosity/Pa·s	$2.46e-05$
kappa_gdl	GDL permeability/m^2	$1e-12$
kappa_cl	Permeability (porous electrode)/m^2	$1e-13$
sigma_gdl	GDL electric conductivity/S·m^{-1}	5000
sigma_cl	CL electric conductivity/S·m^{-1}	5000
sigma_m	Membrane electric conductivity/S·m^{-1}	2
eps_gdl	GDL porosity	0.3
eps_cl	Porous electrodes porosity	1-eps_gdl-eps_l
eps_l	Electrolyte phase volume fraction	0.2
eps_i	Ionomer volume fraction	0.27
cH_2_ref	Hydrogen reference concentration/mol·m^3	56.4
cO_2_ref	Oxygen reference concentration/mol·m^3	3.39
stoich_a	Anode stoichiometry	1.5
stoich_c	Cathode stoichiometry	3
T	Cell temperature/K	343.15
V_cell	Cell voltage/V	0.9
i_cell	Current density/A·cm^2	According to calculate
A_cl	Catalytic layer area/m^2	W_ch ∗ L

Table 5: Conservation equations of 3-D model.

Description	Equations
Mass conservation equation	$\partial\rho/\partial t + \nabla\cdot(\rho\vec{u}) = S_m$
Momentum conservation equation	$(\partial(\rho\vec{u})/\partial t) + \nabla\cdot(\rho\vec{u}\,\vec{u}) = \nabla\cdot(\mu\nabla\vec{u}) + S_{\vec{u}}$
Material conservation equation	$(\partial(\rho Y_i)/\partial t) + \nabla\cdot(\rho\vec{u}Y) = \nabla\cdot(D_i\nabla Y_i) + S_{Y_i}$
Energy conservation equation	$(\partial(\rho T)/\partial t) + \nabla\cdot(\rho\vec{u}T) = \nabla\cdot(k/c_p\nabla T) + S_T$
Proton conservation equation	$\nabla\cdot(\sigma^{\text{eff}}\nabla\varphi_{\text{H}^+}) + S_{\varphi_{\text{H}^+}} = 0$ $S_{\varphi_{H^+}} = \begin{cases} j_a \text{anode CL} \\ j_c \text{cathode CL} \end{cases}$
Electron conservation equation	$\nabla\cdot(\kappa^{\text{eff}}\nabla\varphi_{e^-}) + S_{\varphi_{e^-}} = 0$ $S_{\varphi_{e^-}} = \begin{cases} -j_a \text{anode CL} \\ -j_c \text{cathode CL} \end{cases}$
j_a and j_c [16]	$j_a = ai_{0,a}(C_{\text{H}_2}/C_{\text{H}_2,\text{ref}})^{1/2}((\alpha_a + \alpha_c/\text{RT})F\eta)$ $j_c = -ai_{0,c}\exp[-16456((1/T) - (1/353.15))](C_{\text{O}_2}/C_{\text{O}_2,\text{ref}})\exp(-(\alpha_c F/\text{RT})\eta)$
Diffusion equations of gas components in porous media	$D_i = \varepsilon^{1.5}(1-s)^{r_s}D_i^0(P_0/P)^{\gamma_p}(T/T_0)^{r_t}$
Transmission equation for liquid water	$(\partial(\varepsilon\rho_l s)/\partial t) + \nabla\cdot(\rho_l\bar{v}_l s) = r_w$

Table 6: Expressions for source terms.

Source items	CL	GDL	Membrane	Bipolar plate	Flow field
S_m	$S_{Y_{\text{H}_2/\text{O}_2}} + S_{Y_{\text{H}_2\text{O}}}$	0	0	0	0
$S_{\vec{u}}$	$-(\mu/K_{\text{GDL}})\vec{u}$	$-(\mu/K_{\text{CL}})\vec{u}$	0	0	0
$S_{Y_{\text{H}_2/\text{O}_2}}$	$-(M_i s_i j/nF)$	0	0	0	0
$S_{Y_{\text{H}_2\text{O}}}$	$-M_{H_2O}[(s_i j/nF) - \nabla\cdot((n_d/F)\vec{i}_e)]$	0	$-\nabla\cdot((n_d/F)\vec{i}_e)$	0	0
S_T	$j(\eta + T\text{d}U_0/\text{d}T) + (\vec{i}_e^{\,2}/k_e^{\text{eff}}) + (\vec{i}_s^{\,2}/\sigma_e^{\text{eff}})$	$\vec{i}_s^{\,2}/\sigma_e^{\text{eff}}$	$\vec{i}_e^{\,2}/k_e^{\text{eff}}$	$\vec{i}_s^{\,2}/\sigma_e^{\text{eff}}$	0
$S_{\varphi_{H^+}}$	$-j$	0	—	0	0
$S_{\varphi_{e^-}}$	j	—	0	—	—

Table 7: Symbols and meanings.

Symbol	Meaning	Symbol	Meaning
ρ	Density/(kg·m^{-3})	i_0	Exchange current density/(A·m^2)
ψ	Solving variables	C	Volume molar concentration/(mol·dm^{-2})
t	Time/s	C_{ref}	Reference molar concentration/(mol·dm^{-2})
$\vec{u}$	Velocity vector/(m·s^{-1})	α	Conversion rate of the electrochemical reactions
Γ	Generalized diffusion coefficient/(m^2·s^{-1})	U	Activation potential/V
κ	Thermal conductivity/(W·m^{-1} K^{-1})	T	Temperature/K
σ	Proton conduction rate/(S·m^{-1})	D_i	Coefficient of diffusion
k	Electron conductivity/(S·m^{-1})	n_d	Proton number/electron number
μ	Viscosity coefficient/(kg·m^{-1}·s^{-1})	ε	The initial diffusion coefficient of the components
K_{GDL}	The permeability of the GDL/(m^2·s)	D_i^0	The initial diffusion coefficient of the i components
K_{CL}	Permeation of the catalytic layer (CL)/(m^2·s)	r_s	Saturation index
M_i	Chemical expression	r_p	Pressure factor
S_i	Stoichiometric coefficients of each component	r_t	Temperature exponent
n	The number of electrons	ρ_l	The density of water (kg·m^{-3})
F	Faraday constant/96 485°C/mol	r_w	Condensation rate of water
a	Active reaction area/m^2	s	Phase saturation of water

experimental results can verify the accuracy and feasibility of numerical simulation.

3. Analysis of the Consistence of Intake Flow Rate

Figures 7(a) and 7(b) are, respectively, the iterative situations of the model during the calculation of the 1-D model. It can be seen from this figure that the cathode and anode converge within the 10000th step, which shows that the calculation model has good convergence and effectiveness. Figure 8 shows the distribution of intake airflow of every single cathode and anode. The uneven intake flow distribution of each monomer is both cathode and anode. Among them, the maximum monomer intake flow rate at the anode is $2.87 * 10^{-5}\,\text{m}^3\cdot\text{s}^{-1}$, the minimum is $2.35 * 10^{-5}\,\text{m}^3\cdot\text{s}^{-1}$, and the difference in intake flow rate is $0.52 * 10^{-5}\,\text{m}^3\cdot\text{s}^{-1}$. The maximum monomer intake flow rate of the cathode is

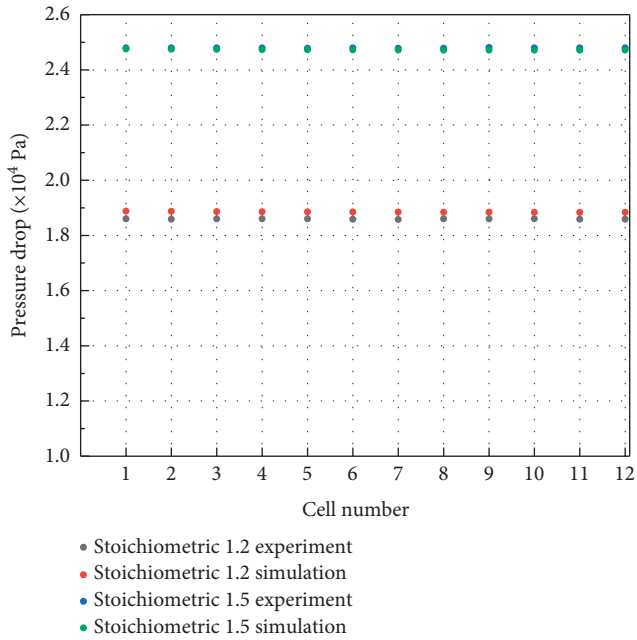

Figure 3: 1-D model verification.

$6.87 * 10^{-5}\,m^3{\cdot}s^{-1}$, the minimum is $5.51 * 10^{-5}\,m^3{\cdot}s^{-1}$, and the difference in intake flow rate is $1.27 * 10^{-5}\,m^3{\cdot}s^{-1}$. The difference in the intake flow rate of the single cell will cause a difference in the performance of the single cell, which will eventually affect the overall performance of the stack. Based on this, the article further optimizes the size of the flow channel to improve the performance of the minimum intake flow rate monomer, thereby enhancing the consistency of the stack.

4. Size Optimization of Monomer Cell

The molecules of the above inlet flow conditions were substituted into the 3D model as boundary conditions for further numerical analysis, and the polarization curves at the highest and lowest inlet flows were obtained, as shown in Figure 9. As shown in Figure 9, the performance difference between the two monomers is noticeable due to the difference in intake flow rate. Moreover, the maximum power density of the maximum intake flow rate monomer is 5.7% higher than that of the minimum intake flow rate monomer. At a current density of $1000\,mA{\cdot}cm^{-2}$, the voltage difference between the two is 0.065 V.

Figure 10 shows the optimization results of channel depth and width. In order to improve the performance of monomer under the minimum intake flow, the width and depth of the channel are optimized in this section, and the width (0.8, 0.85, ..., 1.15,1.2 mm) and depth (0.8, 0.85, ..., 1.15, 1.2 mm) are selected with different size combination; the current density under 0.2V voltage changes with size parameters. The result shows that the current density changes accordingly with the width and depth size, and the current density reaches the maximum when the width and depth are 1.1 mm and 0.8 mm, respectively.

Figure 11 shows the performance comparison between the lowest intake flow rate monomer and the highest intake flow rate monomer after the channel size optimization. As can be seen from the figure, the power density difference between the two monomers is reduced from 5.7% to 2.1%, and the voltage difference is reduced from 0.065 V to 0.035 V at a current density of $1000\,mA{\cdot}cm^{-2}$ after optimization.

According to the optimization of the channel size, the channel size is substituted into the 1-D model, and the distribution diagram of the cathode and anode intake flow rate is obtained. Compared with Figures 12 and 8, it is evident that the intake flow equilibrium of the 80 monomers is significantly improved after the channel size optimization. Specifically speaking, the range of anode flow rate decreased from $0.52 * 10^{-5}\,m^3{\cdot}s^{-1}$ to $0.27 * 10^{-5}\,m^3{\cdot}s^{-1}$ and that of cathode flow rate decreased from $1.27 * 10^{-5}\,m^3{\cdot}s^{-1}$ to $0.58 * 10^{-5}\,m^3{\cdot}s^{-1}$. The improvement of the consistency of intake flow rate will improve the voltage consistency of the stack.

The 80-stack intake flow data before and after the channel size optimization are replaced into the 3-D model to obtain the voltage of each monomer in the stack at $1000\,mA{\cdot}cm^{-2}$. As shown in Figure 13, after the optimization of channel size, the voltage consistency of the stack has been significantly improved.

The voltage difference coefficient is further used to analyze the performance of the stack, the voltage difference coefficient C_v represents the consistency of the cell voltage of the stack, and the calculation formula is

$$C_v = 100 \times \frac{\sqrt{\left[\sum_{i=1}^{N}\left(V_i - \overline{V}/\overline{V}\right)^2\right]}}{n}, \quad (1)$$

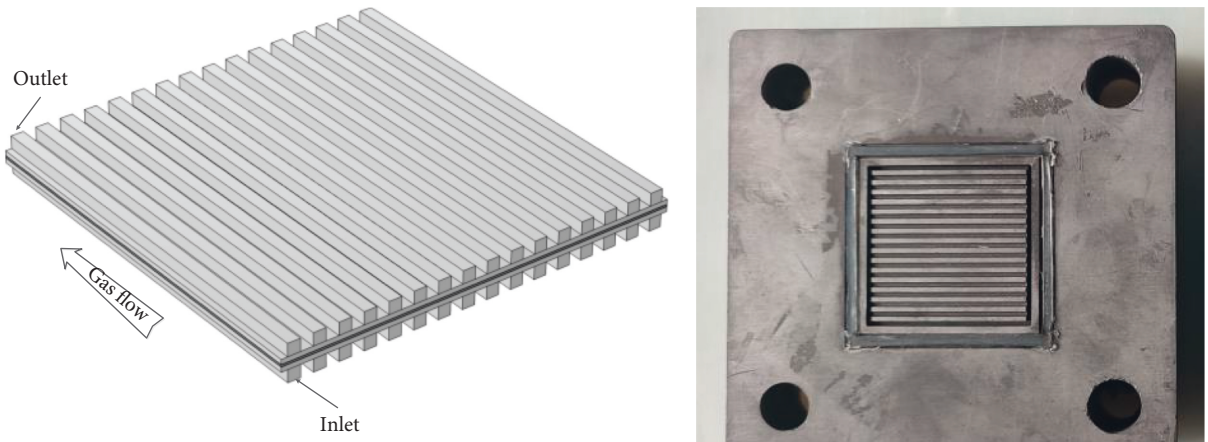

Figure 4: Experimental and simulation models. (a) Simulation cell. (b) Experimental cell.

Table 8: PEMFC experiment parameters.

Parameter	Value
GDL porosity	0.4
GDL thickness/m	$380e-6$
Porous electrode thickness/m	$50e-6$
Membrane thickness/m	$100e-6$
Catalytic layer porosity	0.3
Gas back pressure/MPa	Atmospheric pressure
Anode transfer coefficient	0.5
Cathode transfer coefficient	1
Cell effective area/cm^2	96
O_2 flow rate/ml·min^{-1}	889
H_2 flow rate/ml·min^{-1}	536
Cell temperature/K	343.15
Gas temperature/K	348.15
Dewpoint temperature/K	343.15

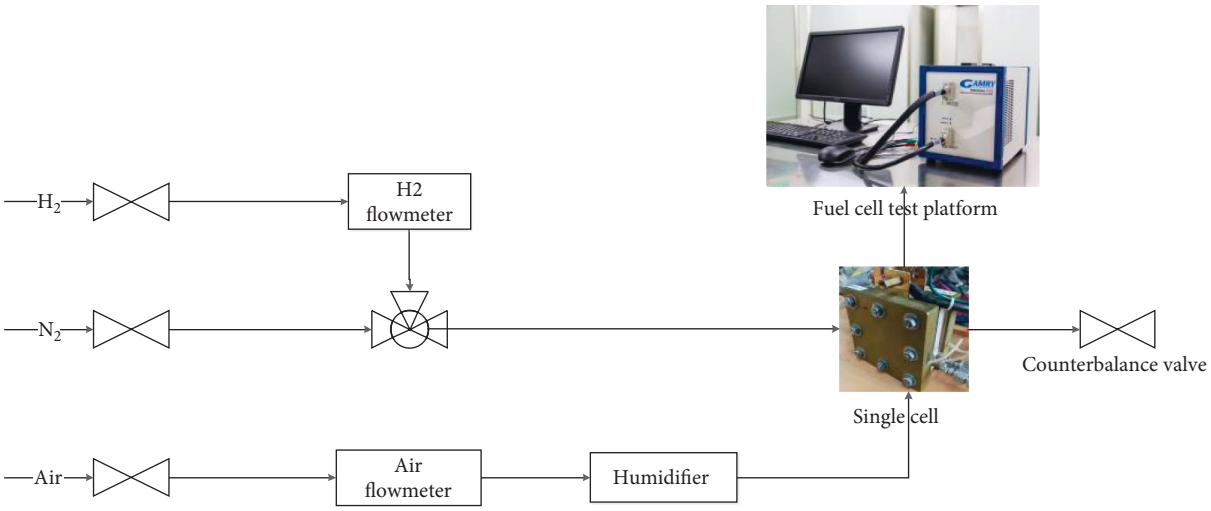

Figure 5: Experimental schematic diagram.

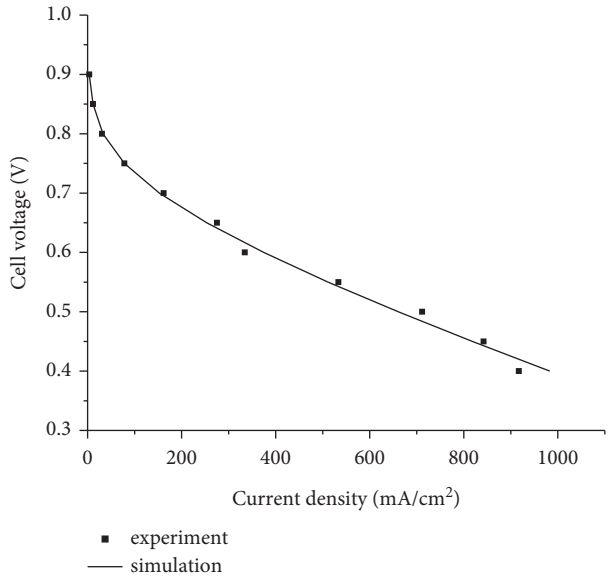

Figure 6: Experimental validation of the model.

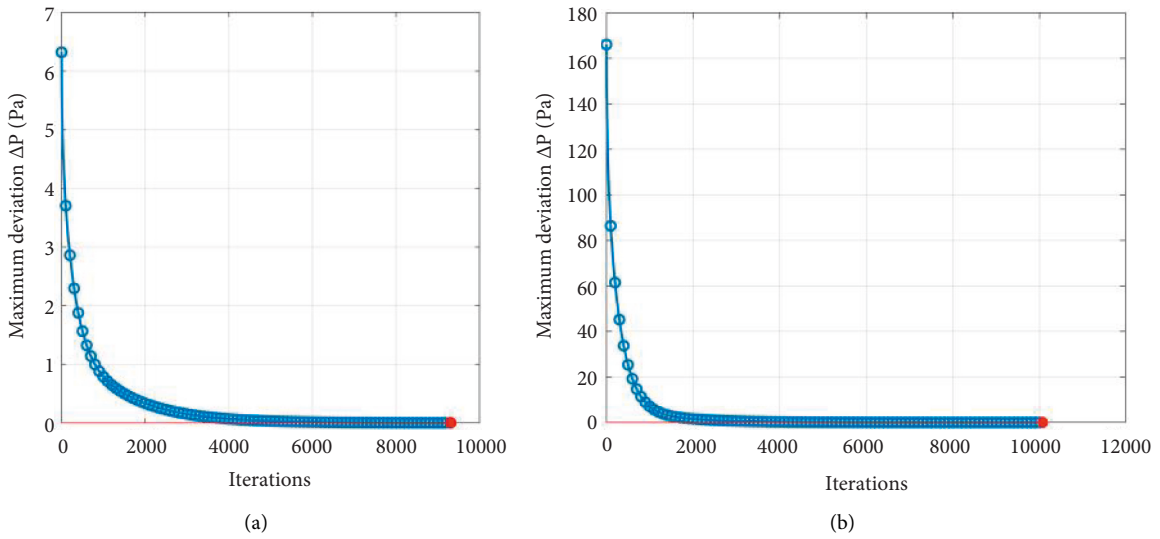

Figure 7: Model iteration times. (a) Anode. (b) Cathode.

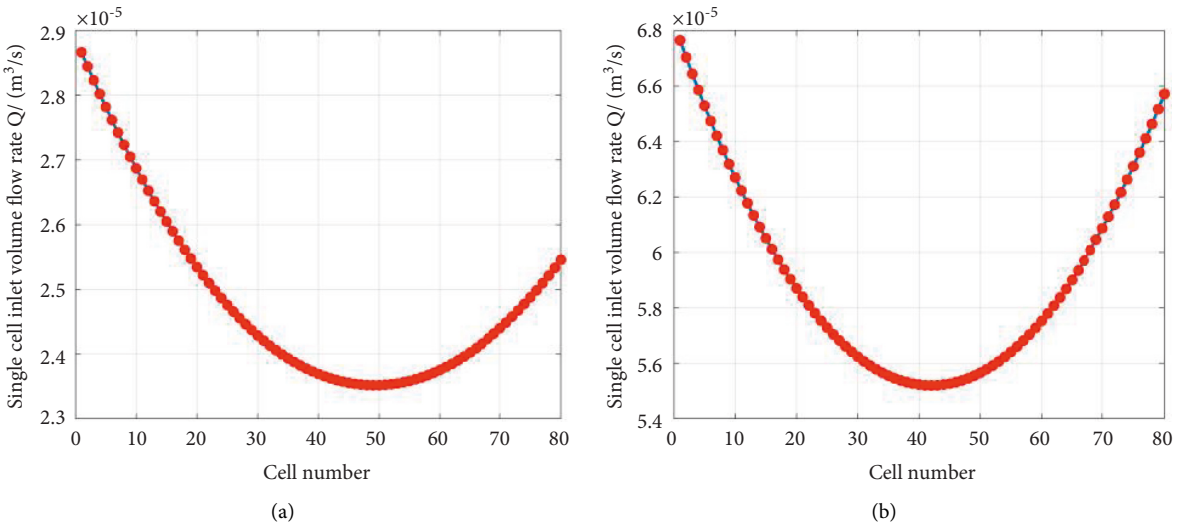

Figure 8: Air intake flow distribution. (a) Anode. (b) Cathode.

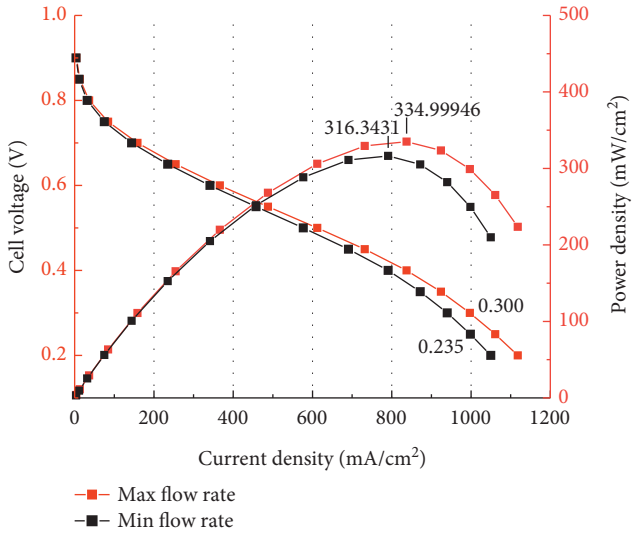

Figure 9: Performance comparison.

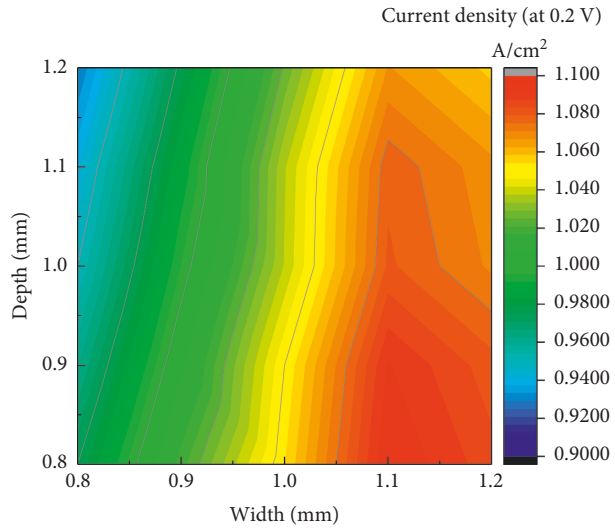

Figure 10: Width-depth optimization.

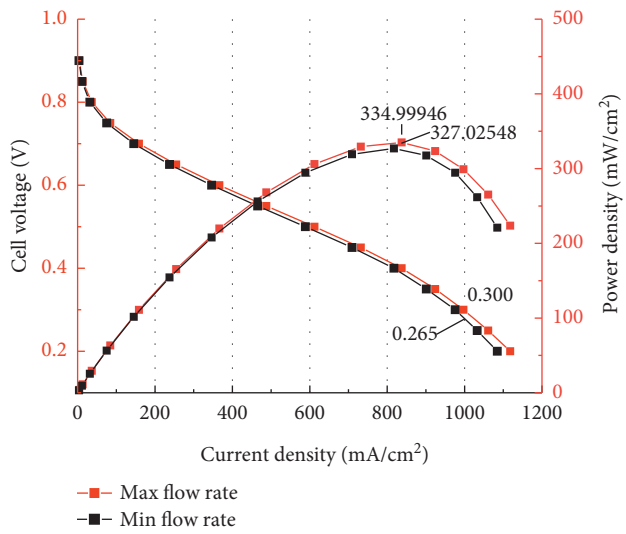

Figure 11: Performance comparison.

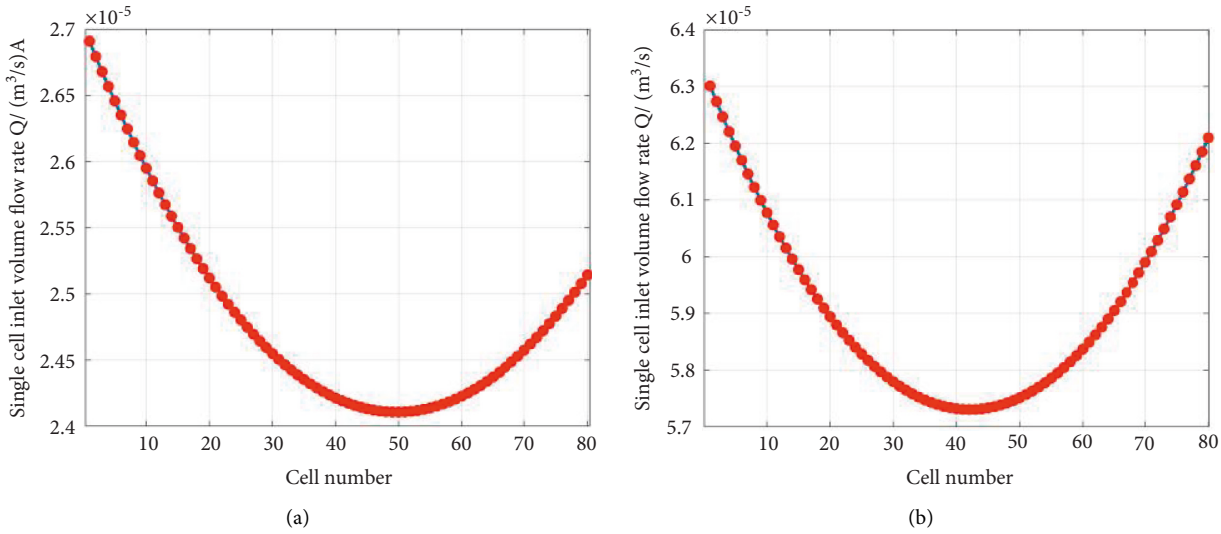

Figure 12: Optimized air intake flow distribution. (a) Anode. (b) Cathode.

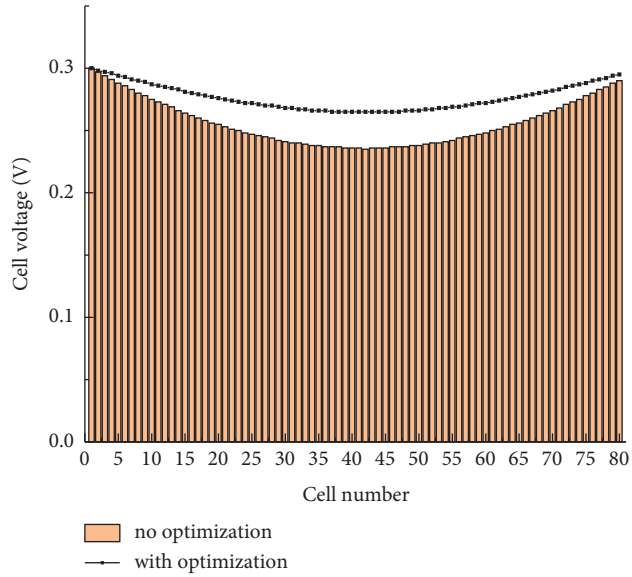

Figure 13: Voltage consistency comparison.

where V_i is the cell voltage, $\overline{V}$ is the average output voltage of the stack, and n is the number of cells.

According to formula (1), C_v changes from 7.21 to 3.70 after optimizing channel size, and C_v is reduced by 48.7%.

5. Conclusion

The article establishes a 1-D flow network model of 80 cell stacks and a three-dimensional steady-state model of a 12 cm ∗ 8 cm PEMFC cell, the performance of the fuel cell is optimized, and the conclusions are as follows.

Experiments were used to verify the accuracy of the 1-D flow network model and the 3-D steady-state model. The convergence of the 1-D model is good. Both the cathode and anode reach confluence within 10,000 steps.

The flow rate distribution of the anode and cathode of the stack is uneven, and the maximum monomer airflow of the anode is $2.87 * 10^{-5}\,m^3{\cdot}s^{-1}$. The minimum is $2.35 * 10^{-5}\,m^3{\cdot}s^{-1}$, and the intake flow rate difference is $0.52 * 10^{-5}\,m^3{\cdot}s^{-1}$. The maximum monomer intake flow rate of the cathode is $6.87 * 10^{-5}\,m^3{\cdot}s^{-1}$, the minimum is $5.51 * 10^{-5}\,m^3{\cdot}s^{-1}$, and the difference in air intake flow is $1.27 * 10^{-5}\,m^3{\cdot}s^{-1}$.

The maximum and minimum intake flow rates obtained from the 1-D model are used as the 3-D model's boundary conditions to calculate the single-cell performance under different intake flow rate conditions. Optimize its performance by changing the minimum intake flow rate monomer's width, depth, and other size parameters. When the width and depth are 1.1 mm and 0.8 mm, respectively, the

monomer performance is the best, and the electrochemical performance is improved.

After the optimization, the extreme difference in the intake flow rate between anode and anode of the stack has been significantly reduced. The consistency of the stack voltage has been considerably improved, and C_v has been reduced by 48.7%.

Data Availability

The datasets used and/or analyzed during the current study are available from the corresponding author on reasonable request.

Conflicts of Interest

The authors declare that they have no conflicts of interest.

Acknowledgments

This study was supported by the Hubei Province Key Research and Development Plan (2021BAA053), the National Shale Oil and Gas Enrichment Mechanism and Effective Development Key Laboratory Fund (20-YYGZ-KF-GC-16), the Key Laboratory Fund of Reservoir Geology and Development Engineering (PLN2020-7), and the National Natural Science Fund (U1762214).

References

[1] Z. Hu, L. Xu, J. Li et al., "A novel diagnostic methodology for fuel cell stack health: performance, consistency and uniformity," *Energy Conversion and Management*, vol. 185, pp. 611–621, 2019.

[2] P. Liu, S. Xu, J. Fu, and C. Liu, "Experimental investigation on the voltage uniformity for a PEMFC stack with different dynamic loading strategies," *International Journal of Hydrogen Energy*, vol. 45, no. 50, pp. 26490–26500, 2020.

[3] H. Sun, C. Xie, H. Chen, and S. Almheiri, "A numerical study on the effects of temperature and mass transfer in high temperature PEM fuel cells with ab-PBI membrane," *Applied Energy*, vol. 160, pp. 937–944, 2015.

[4] P. C. Ghosh, H. Dohle, and J. Mergel, "Modelling of heterogeneities inside polymer electrolyte fuel cells due to oxidants," *International Journal of Hydrogen Energy*, vol. 34, no. 19, pp. 8204–8212, 2009.

[5] A. Jarauta, V. Zingan, P. Minev, and M. Secanell, "A mass transport model for flows in channels and porous media of fuel cells," *ECS Meeting Abstracts*, vol. MA2020-01, no. 40, p. 1804, 2020.

[6] J. Jang, W. Yan, H. Chiu, and J. Lui, "Dynamic cell performance of kW-grade proton exchange membrane fuel cell stack with dead-ended anode," *Applied Energy*, vol. 142, no. 15, pp. 108–114, 2015.

[7] D. Benouioua, D. Candusso, F. Harel, and L. Oukhellou, "PEMFC stack voltage singularity measurement and fault classification," *International Journal of Hydrogen Energy*, vol. 39, no. 36, pp. 21631–21637, 2014.

[8] J. S. Xiong, J. H. Xiao, and M. Pan, "Proton exchange membrane fuel cell flow field simulation and structural size optimization," *Journal of Wuhan University of Technology*, vol. 33, no. 03, pp. 534–536, 2009.

[9] L. Shi, M. G. Zheng, and X. L. Kong, "Effect of cathode flow channel layout on PEMFC performance of snake flow channel," *Power Supply Technology*, vol. 44, no. 02, pp. 68–70+164, 2020.

[10] I. Khazaee and H. Sabadbafan, "Numerical study of changing the geometry of the flow field of a PEM fuel cell," *Heat and Mass Transfer*, vol. 52, no. 5, pp. 993–1003, 2016.

[11] L. P. Wang, L. H. Zhang, and J. P. Jiang, "Optimization of channel dimensions in the flow-field for PEMFC," *Applied Mechanics and Materials*, vol. 44-47, pp. 2404–2408, 2010.

[12] M. L. Wu, Z. Y. Gu, and S. F. Cao, "Design and simulation analysis of the proton exchange membrane fuel cell bipolar plate," *Renewable Energy Energy*, vol. 33, no. 10, pp. 102–107, 2012.

[13] S. Z. Chen, J. Liu, N. Chen, and Y. Wu, "Current status of flow field shape study of PEM fuel cell [J]," *Renewable Energy*, vol. 32, no. 012, pp. 1908–1916, 2014.

[14] A. Kumar and R. G. Reddy, "Effect of channel dimensions and shape in the flow-field distributor on the performance of polymer electrolyte membrane fuel cells," *Journal of Power Sources*, vol. 113, no. 1, pp. 11–18, 2003.

[15] Y. Qin, G. Liu, Y. Chang, and Q. Du, "Modeling and design of PEM fuel cell stack based on a flow network method," *Applied Thermal Engineering*, vol. 144, no. 144, pp. 411–423, 2018.

[16] G. Wang, Q. Zhai, and H. Liu, "Cross self-attention network for 3D point cloud," *Knowledge-Based Systems*, vol. 247, Article ID 108769, 2022.